PRINT ISSN 1119-8362
Electronic ISSN 2659-1499

Full-text Available Online at
https://www.ajol.info/index.php/jasem
https://www.bioline.org.br/ja

J. Appl. Sci. Environ. Manage.
Vol. 28 (3) 823-839 March 2024

Green synthesis of iron (III) oxide (Fe_3O_4) Nanoparticles Using *Citrus sinensis* Peel Extract for the Removal of Ciprofloxacin in Water

[1]FARURUWA, MD; [1,2]*ADAMU, HI; [1]ADEYEMI, MM; [1,3]TOMORI, WB

*[1]*Department of Chemistry, Nigerian Defence Academy Kaduna*
*[2]*Department of Environmental Management Kaduna State University Kaduna.*
*[3]*Federal University of Technology, Akure, Nigeria*

**Corresponding Author Email: habibadamu99@kasu.edu.ng*
**ORCID ID: https://orcid.org/0009-0001-2252-1718*
**Tel: +2348067544793*
Co-Authors Email: mdfaruruwa@nda.edu.ng; mmadeyemi@nda.edu.ng; wbtomori@futa.edu.ng

ABSTRACT: Ciprofloxacin is a widely used antibiotic that can contaminate water sources and pose environmental and health risks. Therefore, the objective of this paper is to explore the green synthesis of iron (III) oxide nanoparticles using *Citrus sinensis* peel extract for the removal of ciprofloxacin in water using standard techniques. The adsorption of ciprofloxacin on the nanoparticles was investigated under different conditions, such as pH, initial concentration of adsorbate, contact time, and different adsorbent doses. The adsorption data were fitted to different isotherm and kinetic models to understand the adsorption mechanism and parameters. The results of characterization revealed the particles to be of nanocrystalline structure with a cubic crystal shape, negative surface charge, and a high thermal stability with elemental composition primarily of Fe and O; it has z- average of 42.60, with Fe-O bond at 693.30cm^{-1} and UV-Visible absorbance at 221nm. The maximum adsorption capacity with ciprofloxacin was 29.21 mg/g (97.45%) at pH of 7 and room temperature of 25 °C. The results of the adsorption data indicated that the adsorption followed the Langmuir isotherm model and the pseudo-second-order kinetic model, suggesting a monolayer adsorption on a homogeneous surface with a finite number of identical sites. The synthesized nanoparticles showed a high efficiency and selectivity for the removal of ciprofloxacin from water, demonstrating it potential as an eco-friendly and low-cost adsorbent for water purification.

DOI: https://dx.doi.org/10.4314/jasem.v28i3.23

Cite this Article as: FARURUWA, M. D; ADAMU, H. I; ADEYEMI, M. M; TOMORI, W. B (2024). Green synthesis of iron (III) oxide (Fe_3O_4) Nanoparticles Using *Citrus sinensis* Peel Extract for the Removal of Ciprofloxacin in Water. *J. Appl. Sci. Environ. Manage.* 28 (3) 823-839

Dates: Received: 18 January 2024; Revised: 24 February 2024; Accepted: 12 March 2024 Published: 29 March 2024

Keywords: nanoparticles, characterization, ciprofloxacin, adsorption.

In recent years, the contamination of water bodies with pharmaceutical compounds has become a significant environmental concern (Thai *et al*., 2023). One of such compounds is ciprofloxacin, a widely used antibiotic in the treatment of sexually transmitted infections, skin, bone, joint infections, prostatitis, typhoid fever, gastrointestinal infections, lower respiratory tract infections, anthrax, plague, and salmonellosis. This antibiotic is frequently detected in wastewater and surface water (Chen *et al*., 2019). The presence of ciprofloxacin in aquatic ecosystems can have detrimental effect on both human health and the environment. It can enter water bodies just like any other pharmaceuticals through various pathways primarily wastewater treatment plants, agricultural run offs, direct disposal of unused medications, and human excretion. (Thai *et al.,* 2023). Several techniques such as the use of activated carbon to adsorb contaminants from pharmaceuticals (mainly aromatic compounds) has recently begun to be studied. (Arvaniti and Stasinakis, 2015). Research over the past few years has shown advanced oxidation processes (AOPs) to be

**Corresponding Author Email: habibadamu99@kasu.edu.ng*
**ORCID ID: https://orcid.org/0009-0001-2252-1718*
**Tel: +2348067544793*

very effective in the degradation of numerous organic and inorganic compounds including pharmaceuticals (Lakshmi and Singh, 2022). Various studies have demonstrated that numerous pharmacologically active compounds can be photodegraded, since they generally contain aromatic rings, heteroatoms, and other functional groups that allow absorption of solar radiation or produce reactions with photosensitizing species that induce their photodegradation in natural water (Sharma *et al.,* 2022). In general, the removal percentages obtained by using UV radiation alone were quite low (lower than 30%), and they reached values around 100% when adding H_2O_2, TiO_2, or TiO_2/activated carbon (Zhang *et al*., 2020). Nanotechnology has emerged as a promising field for addressing various environmental challenges, including water pollution. Among the different types of nanoparticles, iron oxide nanoparticles (IONPs) have gained considerable attention due to their unique properties and potential applications in environmental remediation. IONPs possess high surface area, magnetic properties, and catalytic activity, making them suitable candidates for the removal of organic pollutants from water (Skiba *et al*., 2019; Thi *et al*., 2020; Zayed *et al*., 2022).

However, most of the conventional synthesis method involve high temperature, pressure, energy consumption and toxic chemicals which limit the large-scale production and application of IONPs. Some efforts have been made to develop green synthesis of IONPs using biological and natural sources such as plant extracts, bacteria, fungi, and algae which can reduce the environmental impact and enhance the biocompatibility of IONPs. (Majumder *et al.,* 2019; Priya *et al*., 2021; Ogbezode *et al.,* 2023). The synthesis of IONPs using green and sustainable approaches has garnered significant interest in recent years (Ahmadpour *et al.,* 2019). Utilizing natural extracts as reducing and stabilizing agents offers several advantages over conventional chemical methods (Zayed *et al.,* 2022; Adamu *et al*., 2023). Orange peel extract (OPE) is one of such natural extract that contains various bioactive compounds capable of reducing metal ions and stabilizing nanoparticles. OPE is abundant, cost-effective, and environmentally friendly, making it an attractive alternative for nanoparticle synthesis (Zayed *et al.,* 2022). Therefore, the objective of this paper is to explore the green synthesis of iron (III) oxide nanoparticles using *Citrus sinensis* peel extract for the removal of ciprofloxacin in water using.

MATERIALS AND METHODS

Preparation of orange peel extract: Orange peels (*Citrus Sinensis*) were collected from orange sellers as a waste, washed several times with distilled water to remove dirt, cut into smaller pieces, dried under shade for 7days and grounded in an electric blender (silver crest) into a fine powder. A 10mg of the ground orange peel was accurately weighed using an analytical balance (Adventurer OhausAR310MS-H-S Wincon), into an erlenmeyer flask and the polyphenols content extracted with 150ml distilled water at a temperature of 40°C for 2hr over a magnetic stirrer (500rpm/min; MS-H-S Wincon) (Faisal *et al.,* 2021; Adamu *et al.,* 2023). The polyphenols content of the extracts from orange peel was thereafter determined by Folin-Ciocalteu assay method as described by Kupina *et al*., (2018).

Synthesis of iron oxide (FeO_3) nanoparticles: The iron oxide nanoparticles were synthesized by coprecipitation method, a 100ml of the orange peel extract was measured using a measuring cylinder and transferred into an erlenmeyer flask. The flask was then placed on a magnetic stirrer, a 50ml Fe^{3+} and Fe^{2+} salt solution (molar ratio 2:1) was gradually added into the erlenmeyer flasks. As the reaction proceeded, the pH of the solution was regulated by dropwise addition of a 1M solution of NaOH from the initial pH of 6.3 to attain a pH of 11. The solution was continuously stirred for 1hour using the magnetic stirrer to homogenize for completion of the reaction. The nanoparticles were recovered by separation using a centrifuge at 5000rpm for 10min, it was washed five times with deionized water and finally with ethanol to remove impurities. It was then dried in an oven at 130^0C and stored in an air tight container (Lunge *et al.,* 2014; Yew *et al*., 2016; Mohamed kalith *et al*., 2022). The formation of the nanoparticles was identified by the change in colour of the solution and confirmed using UV-vis spectroscopy.

Characterization of the synthesized iron oxide (Fe_3O_4) nanoparticle: The functional groups on the extract of orange peel and the IONPs were analyzed using Shimadzu Fourier transform Infrared Spectrophotometer- FTIR 8400 S at a wave range of 4000-400cm^{-1}, T70 PG Instruments UV–visible absorption spectrophotometers from 200 to 800 nm were used to monitor the reduction of iron ions to iron oxide nanoparticles. The size of the synthesized metal nanoparticles was measured using Malvern Panalytical Zetasizer multi-AnglScatteringLight Scattering Nano ZS90 according to standard test methods ASTM E11:61 (ASTM Standard Test Method (E11-17) 2017) as described by Hassabo *et al.,* (2023). The surface morphology and elemental compositions were studied with SEMEDS (Scanning Electron microscope model JOEL JSM 7600F). The crystal structure and composition of materials was analysed

with Rigaku MiniFlex 6G XRD machine. The surface area was studied with JW-DA:76502057en China. The thermal stability of the nanoparticles was studied with thermogravimetric analyzer (TGA Q50).

Batch adsorption experiment: The adsorption of ciprofloxacin was studied by batch experiment technique as described by (Ahmadpour *et al.,* 2019). The optimum adsorbent dose was determined by the varying adsorbent dose from 20-100mg, pH between 3, 5.7, 9 and 11, the pH was adjusted using 0.1M of HCl and NaOH. The adsorbate dosage was also varied between 2-10mg/L within a time frame of 5-40mins at a shaking speed of 200rpm. The specific amount of ciproflaxacin adsorbed for the varying experimental condition was calculated from the following equation

$$qe = \frac{(Co-Ce)V}{W} \qquad (1)$$

$$\%\ Removal = \frac{Co-Ce}{Co} * 100 \qquad (2)$$

Where qe is the adsorption amount of ciprofloxacin (mg/g) in the solid at equilibrium; Co and Ce are the initial and equilibrium concentrations of pharmaceutical (mg/L), respectively; V is the volume (ml) of the aqueous solution and W is the mass (g) of adsorbent used in the experiments.

Determination of point of zero charge (pH_{PZC}): The salt addition technique was used to determine the pH_{pzc} of the IONPs as described by Bakatula *et al.,* (2018). Identical amounts of IONPs (0.2g) were added to a set of solutions of of 0.1 M $NaNO_3$ but different pH values. The pH was adjusted with 0.1 M HNO_3 and 0.1 M NaOH as needed to obtain the appropriate pH range of 2, 3, 4, 5, 6, 7, 8, 9, 10, and 11 (±0.1 pH units). The samples were shaken for 24 hours using a rotary agitator at 200 rpm. After settling, the pH values of the supernatant in each tube were measured and denoted as pHf. The point of zero charge (PZC) was obtained from the plot of ΔpH (=pHf – pHi) against pHi.

Kinetic studies: At the optimum conditions studied, adsorption kinetics data was fitted into pseudo first order, pseudo second order and intraparticle diffusion and Elovich kinetics models in order to determine its order and mechanism of adsorption. The applicability of the models will be measured by the regression values (Opotu *et al*., 2022). The pseudo first order kinetic model was studied according to the integrated rate law equation:

$$\ln(qe - qt) = lnqe - K1t \qquad (3)$$

And the pseudo first order (PFO) kinetic model is expressed as

$$\ln(qe - qt) = lnqe - K1t \qquad (4)$$

Where qe and qt (both in mg/g) are the amount of pharmaceutical adsorbed per unit mass of adsorbent at equilibrium and time "t" respectively. The adsorption rate constant (K_1) for pharmaceutical sorption will be calculated from the slope of the linear plot ln (qe- q) vs time (t)

The Pseudo second order kinetic model integrated rate law equation:

$$\frac{t}{qt} = \frac{1}{K_2 q_e^2} + \frac{1}{q_e} \qquad (5)$$

Where qe and qt (both in mg/g) are the amount of pharmaceutical adsorbed per unit mass of adsorbent at equilibrium and time "t" respectively. The adsorption rate constant (K_1) for pharmaceutical sorption will be calculated from the slope of the linear plot ln (qe- q) vs time (t) and K_2 is the pseudo- second order rate constant for sorption determined from the plot of t /qe vs t (lunge *et al.,* 2014).

The intraparticle diffusion kinetic model equation is given by:

$$qt = k_p t^{1/2} \qquad (6)$$

Where qt is the amount of adsorbate per unit mass of adsorbent at time t (mg/g), Kp is the intraparticle diffusion rate constant (mg/g $min^{1/2}$, t is the time (min), and C which indicates the boundary layer effect is the intercept (mg/g), (Ramírez-Rodríguez and Castillo-Alvarado, 2012). The data was plotted as qt versus $t^{1/2}$, which gives a straight line according to the intraparticle diffusion kinetic model equation.
The Elovich kinetic model equation is given by:

$$qt = \frac{1}{\beta}\ln(\alpha\beta) + \frac{1}{\beta} lnt \qquad (7)$$

Where qt is the amount of adsorbate per unit mass of adsorbent at time t (mg/g), α is the initial adsorption rate (mg/g min), β is the desorption constant (g/mg), and t is the time (min). The data was plotted as qt versus lnt, which gives a straight line according to the Elovich kinetic model equation. The values of α and β can be calculated from the intercept and the slope, respectively. The coefficient of determination (R^2) can be used to measure the quality of the fit.

Adsorption isotherm: In order to understand the adsorption mechanism and to compute various

adsorption parameters three isotherm models namely Langmuir, Freundlich will be used to interprets the experimental data

The equation of the Langmuir isotherm, which suggests a monolayer adsorption onto a surface (Oputu *et al.*, 2022), is given below.

$$qe = \mathrm{qmax}\frac{\mathrm{KLCe}}{1} + \mathrm{KLCe} \qquad (8)$$

The Langmuir's isotherm was transformed into its linear form, as represented in Eq. (4), to determine the adsorption parameters

$$\frac{1}{qe} = \frac{1}{KLqmax}.\frac{1}{Ce} + \frac{1}{qmax} \qquad (9)$$

Where KL is the Langmuir constant (L/mg) and qmax is the maximum amount of the pharmaceutical adsorbed per gram of adsorbent at equilibrium (mg/g) and $C\,e$ is concentration of adsorbate at equilibrium (mg g−1). A plot of 1/ qe against 1/Ce produces a straight line whose slope and intercept are used to determine values of Langmuir constants qmax and KL

The essential characteristic of the Langmuir isotherm can also be expressed by a dimensionless constant called the separation factor RL (Ayub *et al*., 2020). Also, it is used to predict the adsorption efficiency of the process, the dimensionless quantity (RL) can be calculated using the following equation

$$RL = \frac{1}{1+KLC0} \qquad (10)$$

Where KL is Langmuir constant (mg/l) and Co is initial concentration of adsorbate (mg/l); RL values indicate the adsorption to be unfavorable when RL>1, linear when RL<1, favorable when 0 < RL < 1 and irreversible when RL=0

The equation of the Freundlich isotherm, which suggests that the adsorption occurs onto a heterogeneous surface(Oputu *et al.*, 2022), is as follows.

$$logqe = \log Kf + \frac{1}{n}logCe \qquad (11)$$

where KF and n are the isotherm constants that indicate the capacity and intensity of the adsorption, and 1/n is a function of the strength of adsorption(Al-musawi *et al*.,2021). The plot of log(qe) against log(Ce) produces a line with intercept value of KF and the slope of 1/n.

A value of 1/n >1 suggests weak adsorption while 1/n < 1 suggests strong adsorption bond as a result of strong intermolecular attraction within the adsorbent layers. When the value of n ranges from 2 and 10, indicates good adsorption when the value of n is between 1- 2, it indicates moderate adsorption capacity and less than one indicating undesirable adsorption capacity (Hamdaoui and Naffrechoux, 2007)

Temkim isotherm model which takes into account the effect of indirect adsorbate/adsorbate interaction on the adsorption process is also assumed that the heat of adsorption (DH_{ads}) of all molecules in the layer decreases linearly as a result of increase surface coverage.(Piccin *et al.*, 2011)

The linear form of Temkin isotherm model is given by the following

$$qe = \frac{RT}{b}lnKT + \frac{RT}{b}lnCe \qquad (12)$$

Where KT is the equilibrium binding constant (L mol^{-1}) corresponding to the maximum binding energy, b is related to the adsorption heat, R is the universal gas constant (8.314 J K−1 mol^{-1}) and T is the temperature (K). Plotting qe versus ln (Ce) produces a straight line of slope RT/b and intercept (RT ln KT)/b (Piccin *et al.,* 2011)

RESULTS AND DISCUSSION

Polyphenol contents and FTIR Characterization of the orange peel extract: Based on the Folin-Ciocalteu assay of the orange peel extract, the polyphenol content was 33.40 mg GAE/g. These polyphenols can play a crucial role in the synthesis process by facilitating the reduction of iron and promoting the formation of iron oxide nanoparticles as well as providing better protection against oxidation or degradation of the synthesized iron oxide nanoparticles. The antioxidant activity of the extract can also enhance the stability and shelf life of the nanoparticles, making it more suitable for various applications (Lamuela-Raventós, 2018). The orange peel extract shows C=C bending vibration of alkene at 998.90 (Figure 1). In the synthesis of iron oxide nanoparticles alkenes can donate electrons to the iron ions (Fe^{3+}) and reduce them to form iron oxide nanoparticles (Fe_2O_3 or Fe_3O_4) (Kumar *et al*., 2007). The reduction process can be influenced by factors such as the type, length, and branching of the alkane or alkene chain. For example, a longer and more alkene chain can result in a faster reduction rate and smaller nanoparticle size (Latif *et al*., 2019). Alkanes, alkenes and alkynes can also bind to the surface of the iron oxide nanoparticles and prevent them from agglomeration or oxidation (Ahmadi *et al*., 2021). The

capping process can also be influenced by factors such as the type, length, and branching of the alkane or alkene chain. For example, a longer and more branched alkane or alkene chain can result in a stronger capping effect and higher stability of the nanoparticles (Gan *et al*., 2012). A more unsaturated alkene chain can also increase the reactivity of the nanoparticles aside from the capping effect (Fahmy *et al.,* 2018; Priya *et al*., 2021; Jeevanandam *et al.,* 2022).

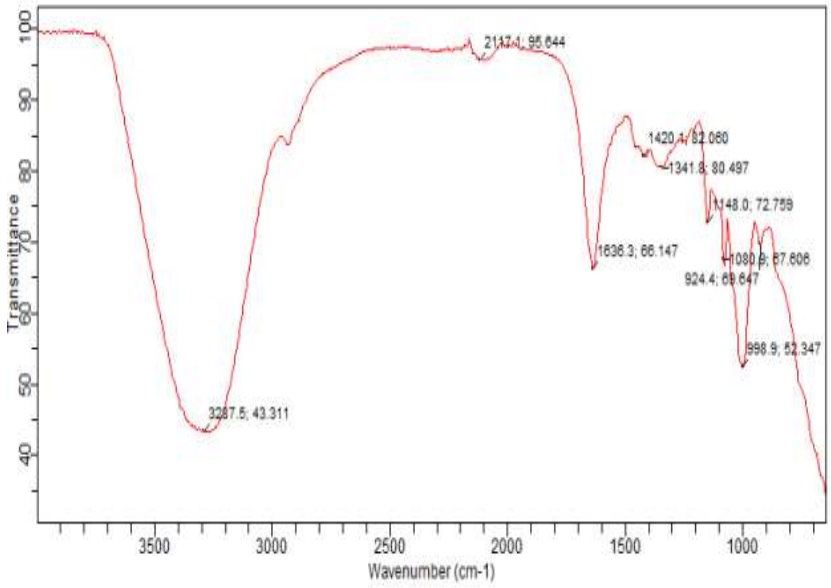

Fig 1: FTIR spectrum of orange peel extract

Peaks at 1148 correspond to C-O stretching vibrations of ethers. Ethers are compounds that have an oxygen atom (-O-) linking two carbon chains (Bashir *et al*., 2020; Priya *et al*., 2021). These compounds can act as both reducing and capping agents in the green synthesis of iron oxide nanoparticles. As reducing, ethers can donate electrons to the iron ions (Fe^{3+}) and reduce them to form iron oxide nanoparticles (Fe_2O_3 or Fe_3O_4). Similarly, peaks at 1341.90 correspond to O-H bending vibration of Phenols and 1080.90cm^{-1} correspond to O-H bending vibration of alcohols. Phenols and alcohols can donate electrons to the iron ions (Fe^{3+}) and reduce them to form iron oxide nanoparticles (Fe_2O_3 or Fe_3O_4) (Fahmy *et al*., 2018; Salgado *et al*., 2019; Nawaz *et al*., 2023). Also, the peaks at 3287.50cm^{-1} correspond to presence of carboxylic acid functional group in the extract of orange peel. During the synthesis of iron oxide nanoparticles carboxylic acid can reduce the iron ions (Fe^{3+}) to form iron oxide nanoparticles (Fe_2O_3). This process is also known as bioreduction. This agrees with the findings of Yew *et al*., (2016) in the synthesis of (Fe_3O_4) nanoparticles using seaweed, the study attributed the functional groups of seaweed as the reducing agents as well as stabilizers and capping agents in the synthesis of Fe_3O_4–NPs. Carboxylic acid can also act a capping agent, it can form a protective layer around the iron oxide nanoparticles and stabilize them in the aqueous solution. This process is also known as biofunctionalization (Fahmy *et al*., 2018 Jeevanandam *et al*., 2022). However, the underlying mechanism of the bioreduction of metal ions by biomolecules is still not confirmed but from scientific report, it has been assumed that functional groups such as -COOH, O-H, C-O-C, C=C, -CHO etc plays important roles in the reduction of metal ions as reported in literatures (Jeevanandam *et al*., 2016; Ishak *et al*., 2019). Overall, Orange peel extract is a rich source of phenolic compounds, which are organic molecules that contain one or more hydroxyl groups attached to an aromatic ring. Phenolic compounds have various biological activities some of which include Flavonoids, Phenolic acids and Limonoids (Erukainure *et al.,* 2016; Shehata *et al*., 2021).

Characterization of the synthesized iron oxide nanoparticles: The UV-Visible spectroscopy analysis of iron oxide nanoparticles synthesized from orange peel extract showed adsorption at 368 nm. This implies that the nanoparticles have a band gap energy of about 3.37 eV, which corresponds to the visible light range. The band gap energy is the minimum energy required to excite an electron from the valence band to the conduction band in a semiconductor material. The band gap energy can be calculated by using the formula $E = hc/\lambda$, where E is the energy, h is the

Planck's constant, c is the speed of light, and λ is the wavelength (Khan *et al*., 2022). The adsorption peak at 368 nm indicates that the iron oxide nanoparticles have a nanocrystalline structure and a small size (Alangari *et al*., 2022). The size and shape of nanoparticles can affect their optical properties and band gap energy. Smaller nanoparticles have larger band gap energies and higher adsorption peaks than larger nanoparticles. The shape of nanoparticles can also influence the distribution of electrons and the density of states in the valence and conduction bands (Nawaz *et al*., 2023). The UV-Visible absorption wavelength of iron oxide nanoparticles synthesized from plant extracts may vary depending on the type of plant extract and the synthesis conditions (Batool *et al.,* 2021). However different wavelength of adsorption has been reported in literature for different plant extracts such as 277 nm for iron oxide nanoparticles synthesized using *Murraya koenigii* leaf extract by Mohanraj *et al*., (2014), 295-301 nm for iron oxide nanoparticles synthesized using Avicennia marina flower extract by Karpagavinayagam and Vedhi (2019), 450 nm for iron nanoparticles synthesized using *Phoenix dactylifera* extract by Batool *et al.,* (2021). The Orange Peel Extract synthesized iron oxide nanoparticles showed an average hydrodynamic diameter, represented by the Z average of 42.60 nm with a Polydispersity Index (PDI) of 0.547. This indicates a relatively broad size distribution of the particles suggesting the presence of particles with varying sizes (Figures 2 and 3). The availability of polyphenols with different reducing properties found in aqueous plant plays vital roles in the size distribution of the iron oxide nanoparticles (Checkouri *et al*., 2020). The size distribution and polydispersity index of nanoparticles is also a function of different conditions or functions such as the refractive index of solvent, nature of dispersive medium, mean sizes of the nanoparticles and the method of synthesis employed (Gaumet *et al*., 2008).

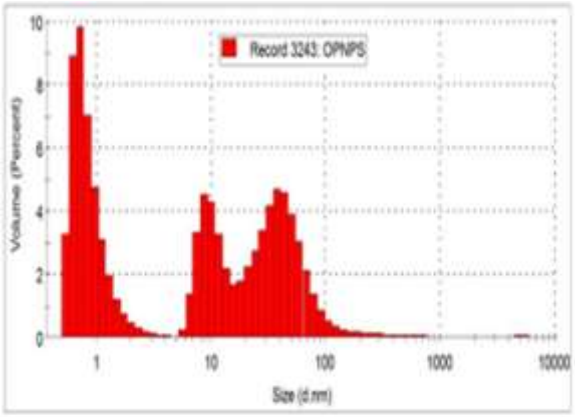

Fig 2: Size distribution of OPNPs against volume

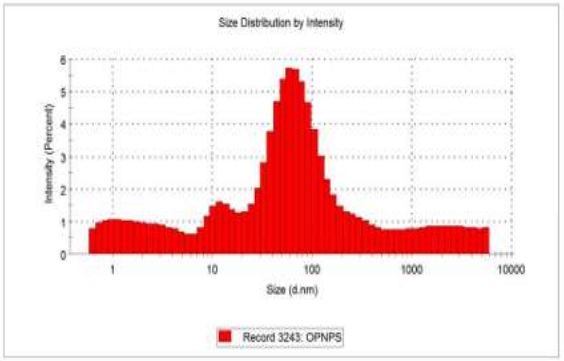

Fig 3: Size distribution of OPNPs against intensity

The TGA analysis of the synthesized iron nanoparticles is presented on Figure 4, the OPNPs sample was heated under a condition of static air at a heating rate of 5°C/ min, it showed a slight weight loss of 0.30% when heated from 0-98°C, this observed weight losses is attributed to evaporation of water present in the synthesized nanoparticles (Bashir *et al.,* 2020; khan *et al.,* 2022). Further weight loss was observed with continuous heating as the OPNPs showed a weight loss of 31.70% between the heating temperature of 250- 340°C.The observed weight losses could be attributed to decomposition of hydroxyl group and other organic compound such as the polyphenols or stabilizers used as the reducing and stabilizing agents during the synthesis remaining in the sample (Bashir *et al*., 2020; khan *et al..,* 2022). As the sample is heated, these compounds are burned off resulting in weight loss.

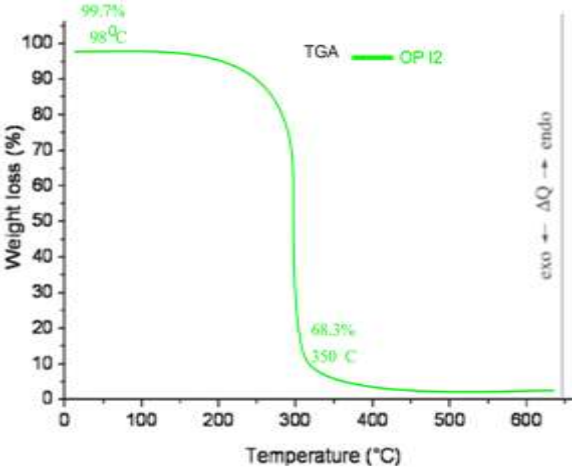

Fig 4: Thermogravimetric analysis of OPNPs

As observed on the Fig. 4, all the synthesized NPs where heated within the temperature range of 0-600°C. The NPs showed no further decomposition at temperatures from 450°C for OPNPs. However, the particles showed no further decomposition nor loss in

weight when heated up to 600°C.Hence, the synthesized nanoparticles were calcined at a temperature of 450°C before further characterization. The FTIR of the orange peel extract synthesized NPs (OPNPs) showed 8 major adsorption peaks as presented in Figure 5. The absorption peaks at 3235.32 and 1066.00 cm^{-1} were attributed to the typical O-H stretching vibration of carboxylic acid and primary alcohol respectively, these peaks are a shift from the 3287.50cm^{-1} and 1080.90cm^{-1} observed in the FTIR analysis of the orange peel extract respectively, whereas C=C stretching and bending vibration were identified at 1602.73cm^{-1} and 969.10cm^{-1} which are also a shift from the peak at 1636.30cm^{-1} and 998.90cm^{-1} observed in the orange peel extract while the peak at 2109.67cm^{-1} correspond to and C≡C stretching vibration of alkyne. Additionally, an absorption peaks including C-H stretching vibration at 1077.85 cm^{-1} and 1371.66 cm^{-1} of sulfonate were observed. The presence of O-H and C=C were believed to have acted as reducing agent for ferric/ferrous chloride solution as indicated by the change of colour during the synthesis (Yau *et al*., 2017; Zambri *et al*., 2019). Also, the additional peak at 693.30 corresponding to Fe-O stretching vibration confirms the formation of iron oxide nanoparticles which is similar to the band at 677cm^{-1} reported as Fe-O stretching vibration by Bashir *et al*., (2020) which also correspond to the reported range of 400-850cm^{-1} for metal oxygen bond (Karpagavinayagam *et al*., 2019). It also agrees with the findings of Karpagavinayagam and Vedhi, (2019) for iron oxide nanoparticles synthesized from *Avicennia marina* flowers. the formation of Fe-O was observed at a band of 618 and 467cm^{-1} respectively. Adsorption band at 555 and 435cm^{-1} were also reported by Miri *et al*., (2021) as vibrational band of O-Fe-O and Fe-O respectively.

The surface morphology of the nanoparticles at the different magnifications of 8000, 9000 and 10000 as studied using SEM (Plate. 1) shows a non-uniform irregular shape, at magnification of 8000, it appears with a smooth surface however, the surfaces are rough and also non uniform indicating iron oxide nanoparticles (Fe_3O_4) aggregation. This agrees with the result obtained in DLS analysis of a PDI of 0.547. The aggregation of the nanoparticles is likely caused by the dipole- dipole interaction of the particles (Da'na *et al.,* 2018). This finding is also similar to nanoparticles synthesized using Simarouba Glauca Leaf Extract by Suby *et al*., (2022); Sudhakar *et al*., (2022). The size of the nanoparticles as calculated using the imageJ software shows size ranges between 7.05-44.18nm with an average of 22.92nm, these values are lower than the values obtained from the DLS analysis but within the reported range. Elemental analysis of the OPNPs with Energy Dispersive X-ray Spectroscopy (EDS) showed a significant emission energy at 2 KeV correspond to the binding energy of Fe (78.65%), at 0.1 KeV for binding energy of oxygen (20.02%) and a small profile at 0.5 KeV corresponding to binding energy of carbon (2.22%) (Figure 6).

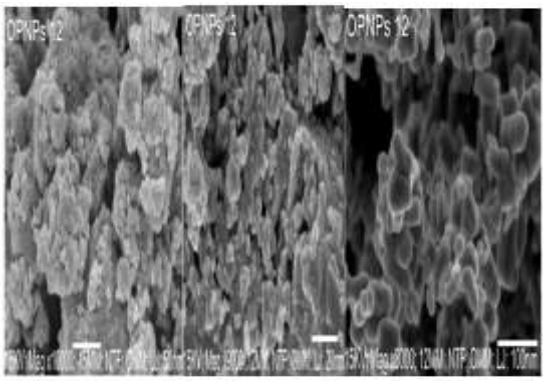

Plate 1: SEM image of OPNPs

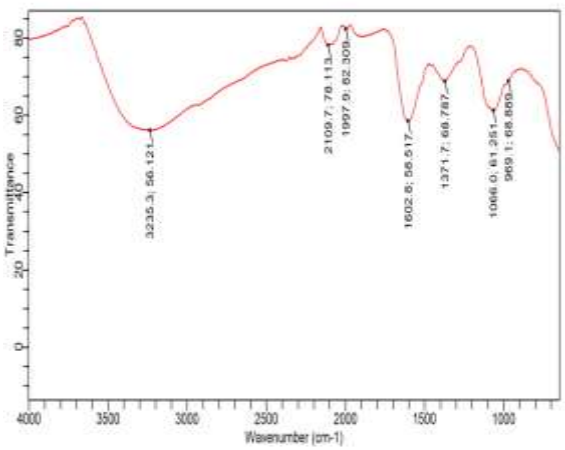

Fig 5: FTIR spectrum of OPNPs

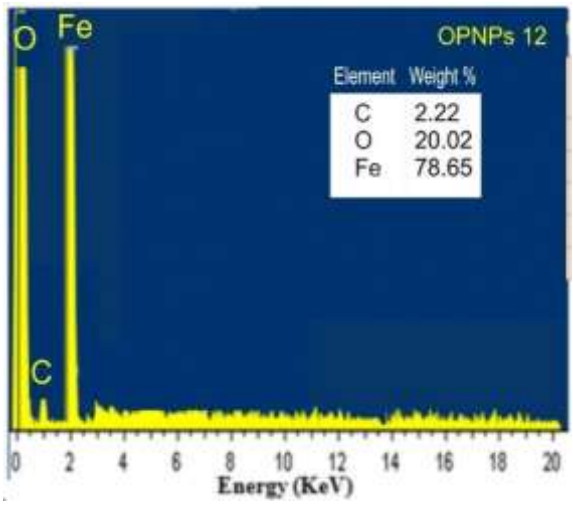

Fig 6: EDS result of OPNPs

X-Ray Diffraction (XRD) analysis is a widely used characterization technique for studying the crystallographic structure of materials, especially nanoparticles. The iron (III) oxide nanoparticles synthesized from orange peel extract as presented on Figure 7 showed distinct diffraction peaks with 2θ values of 30.48, 35.78, 43.34, 53.60, and 63.22 degrees. The most intense peak was observed at 2θ value of 35.78 degrees with an intensity count of 100% magnetite (Fe_3O_4). The peaks indicate that the magnetite was well crystallized (Paul *et al*., 2022). These peaks corresponded to specific crystallographic planes with the HKL values of 022, 113, 004, 224, and 044. The XRD pattern matched well with the ICSD collection code: 77592, reference code 98-006-1958 and also with the PDF data for Fe_3O_4 with ICSD 01–071–6339 reference code. The crystal structure was determined to have a cubic crystal system and a space group of FD-3M. The crystal size was estimated using the Derby Scherrer equation ($D = K\,\lambda / (\beta * \cos\theta)$) where K is the shape factor with a typical value of 0.9; β (2θ) is the full width at half-maximum (FWHM) of a particular diffraction peak in radians; λ is the X-ray wavelength (for copper, λ =1.5406 Å), and θ is the Bragg angle.

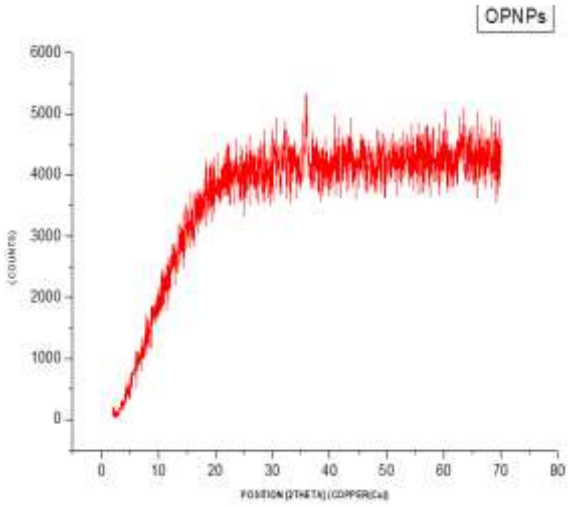

Figure 7: X-ray diffractogram of OPNPs

The calculated crystal size was 45.91nm, which confirmed the synthesis of nanoparticles within the nanoscale range. This value was consistent with the DLS analysis that gave a Z- average of 42.60nm. However, the value was much higher than the calculated size from the SEM image of 22.92nm with a range of 7.05-44.18nm. All the analyses confirmed the synthesis of iron oxide nanoparticles in the nanoscale range. The XRD analysis was in agreement with several similar studies that synthesized iron oxide nanoparticles via coprecipitation such as Jadoun *et al.,* (2021); Paul *et al*., (2022); Arief *et al*., (2023). Brunauer–Emmett–Teller (BET) analysis of the OPNPs showed an extremely high BET surface area of 925.2m^2/g and a Langmuir surface area of 60.52 m^2/g. This suggests that OPNPs is porous and have an irregular shape and size distribution, this agrees with the result of the DLS analysis on Fig 3 and 4 The exceptionally high surface area of the synthesized nanoparticles might be attributed the presence of organic compounds found in orange peel extracts which served as capping agents or stabilizers during the synthesis process, leading to the formation of rough surfaces on the nanoparticles (Thi *et al*., 2020; Lakshminarayanan *et al.,* 2021). This increased surface roughness further contributes to the overall high surface area. However, the nanoparticles may possess inherent porosity, either through the extracts themselves or through the synthesis process (Pershina *et al*., 2020). The presence of pores within the nanoparticles provides additional surface area for gas adsorption, resulting in a higher BET surface area. The coprecipitation method itself allows for a fast nucleation and growth of iron oxide nanoparticles under alkaline conditions, which can produce nanoparticles with high crystallinity and surface area (LaGrow, *et al*., 2019). The BET and Langmuir surfaces of all the synthesized nanoparticles in this study were much higher than those synthesized by Lakshminarayanan *et al*., 2021 using *Bauhinia tomentosa* leave extract (BET surface area of 160.54 m^2/g) and banana peel extract (BET surface area of 97.6 m^2/g); seed extract of Syzygium cumini (Priya *et al*., 2021) with a BET surface area of 89.6 m^2/g. The different properties of iron oxide nanoparticles synthesized using different extracts may affect their applications in various fields, such as catalysis, drug delivery, magnetic resonance imaging, etc (Cheah *et al*., 2021). For example, higher porosity may enhance the adsorption capacity and catalytic activity of iron oxide nanoparticles, while lower porosity may improve their stability and biocompatibility (Cheah *et al*., 2021). Hence, the synthesized nanoparticles are suitable for application in the adsorption of pharmaceuticals in water (Lakshminarayanan *et al.,* 2021

Batch adsorption experiments: Effect of contact time and adsorbent dosage: The maximum adsorption of 81.75% was achieved at 20 minutes for an adsorbent dose of 20mg/50ml, 92.48% at 30 minutes for an adsorbent dose of 40mg/50ml and 91.23% at 25 minutes for an adsorbent dose of 60mg/50ml (Figure 8). For both the 20mg/50ml and 40mg/50ml adsorbent doses, continuous stirring resulted in a steady decline in the amount of CIP adsorbed. However, for the 60mg/50ml dose, there was only a slight decrease in the amount adsorbed. This observation can be due to

saturation, after reaching maximum adsorption, the adsorbent may become saturated with the adsorbate (CIP) molecules. Once the active sites on the adsorbent surface are occupied, further adsorption becomes limited, resulting in a decline in efficiency (Alwared *et al.,* 2021). Also, as the concentration of CIP decreases in the solution during the adsorption process, diffusion limitations can come into play. The transport of CIP molecules from the bulk solution to the adsorbent surface may become slower, reducing the overall efficiency of adsorption (Liu *et al*., 2017). At an adsorbent dose of 80mg/50ml, the efficiency of CIP adsorption increased continuously and reached equilibrium at 40 minutes with an efficiency of 91.23%**.** At higher adsorbent doses, there are more active sites available for CIP molecules to interact with, leading to more efficient adsorption (Al-musawi *et al*., 2021). Additionally, the increased number of adsorbent particles can create a more favorable environment for CIP molecules to interact with the surface leading to the continuous increase in adsorption (Mohammed *et al*., 2019; Adamu *et al*., 2023). For an adsorbent dose of 100mg/50ml, the efficiency increased to 94.57% at 10 minutes and remained fairly stable throughout the experiments. This suggests that this particular adsorbent dose is highly efficient at removing CIP from aqueous solutions. Hence, the optimum adsorbent dose and contact time is 100mg/50ml and 10minutes respectively depending on the specific experimental conditions and the desired level of efficiency. These observations suggest that the efficiency of CIP adsorption is influenced by both contact time and adsorbent dose.

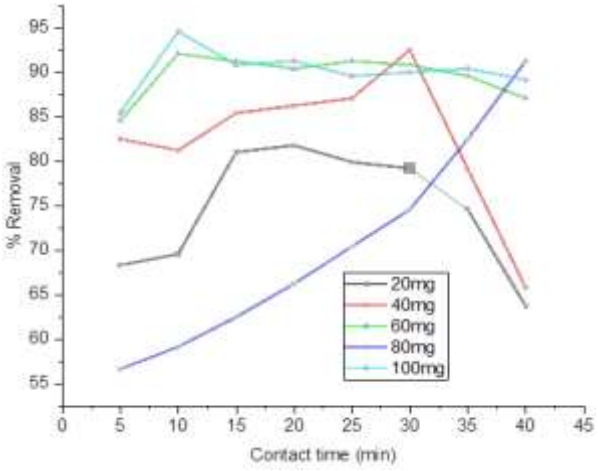

Fig 8: Result of the effect of contact time on the removal Ciprofloxacin with IONPs

Effect of initial concentration: The result shows an increase in the adsorption of the CIP from 2-6mg and stabilized as the concentration increased (Fig 9). The maximum adsorption was observed at an adsorbate concentration of 4mg/l which is the optimum adsorbate concentration for the experiment. These observations suggest that the efficiency of CIP adsorption is influenced by the initial concentration of adsorbate. However, the reasons for increase in adsorption of CIP with increase in initial concentration may depend on the specific experimental conditions and the characteristics of the adsorbent used (Liang *et al.,* 2023). But generally, it is expected that increasing the initial concentration of adsorbate would lead to more favorable interactions between CIP molecules and active sites on the adsorbent surface. This will result in a more efficient adsorption and higher overall efficiency (Al-Musawi *et al*., 2021; Wakejo *et al*., 2022).

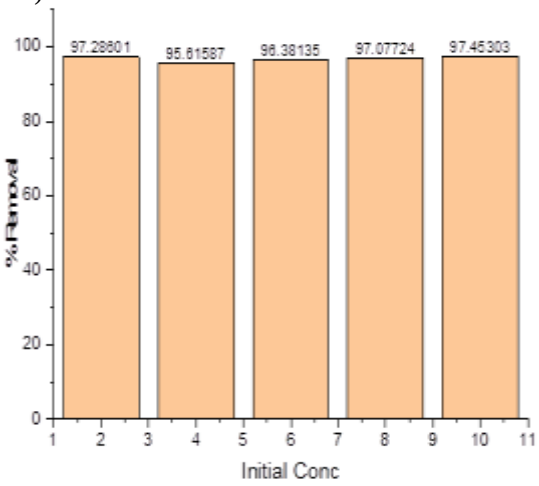

Fig 9: Effect of initial concentration of Ciprofloxacin on it removal from water using IONPs

pH_{pzc} analysis and Effect of pH on the removal of ciprofloxacin from water using IONPs: The adsorption process is influenced by the pH-dependent charge of the sorbent and sorbate species (Garau *et al*., 2019). At different pH values, the surface charge of the sorbent can change, affecting its affinity for sorbate species. Similarly, the binding nature of sorbate can be influenced by pH, as it can alter the ionization state and speciation of sorbate molecules. These changes in surface morphology and binding nature can impact the efficiency and capacity of adsorption processes (Garau *et al.,* 2019; Badawi *et al*., 2021). Figure 10 and 11 presents the plots of the pH_{pzc} experiments and the effect of pH on the removal of ciprofloxacin from water using the OPNPs. As shown in Figure 10, the pH_{pzc} was determined to be slightly acidic (pH=6.9). The implication is that the IONPs surface will be covered with OH^- negative charges at the solution pH>6.9, while at pH<6.9, the surfaces will be covered with H^+ positive charges. Ciprofloxacin is a zwitterionic molecule possessing both positive and negative charges (Uruén *et al*.,

2020). The carboxyl group in ciprofloxacin has a pKa of 6.09, while the secondary amino group has a pKa of 8.74 (National Center for Biotechnology Information, 2023). At pH values above 8.7, ciprofloxacin molecules are negatively charged, while at pH values between 6.1 and 8.7, they are positively charged (Uruén *et al.,* 2020). Hence, the interaction between the IONPs (adsorbent) and the ciprofloxacin (adsorbate) molecules is expected to experience highest attraction between the pH 6.1-8.7 due to the opposing charges of the surfaces (Al-Musawi *et al.,* 2021). Therefore, the effect of pH at 3, 5, 7, 9 and 11 was studied at initial adsorbate concentration of 4mg/l of ciprofloxacin, adsorbent dose of 100mg/50ml, contact time of 10min, and shaking speed of 200rpm. The initial pH of the adsorption system plays a significant role in the adsorption of sorbate, as it affects the surface morphology of the sorbent and the binding nature of sorbate (Song *et al*., 2020). The result as presented on Figure 11 revealed the efficiency of adsorption as low at acidic pH of 3 and basic pH of 9 and 11. The maximum adsorptions (87.89 and 94.57%) were observed at pH of 5 and 7. At these pH range, the surface of the adsorbent and the adsorbate have opposing charges making it suitable for adsorption as described in the pH_{pzc} analysis presented on Fig. 10. Similarly, the OPNPs used in the experiment might have a specific surface charge that affects its interaction with the adsorbate (the substance being adsorbed). At acidic pH values, the surface charge of the adsorbent may become more positive, leading to repulsion between the adsorbent and the adsorbate (Aigbe *et al*., 2022). Similarly, at basic pH values, the surface charge of the adsorbent may become more negative, hindering the adsorption process (Busetty, 2019). Hence, the low adsorption at pH below 5 and above 7.

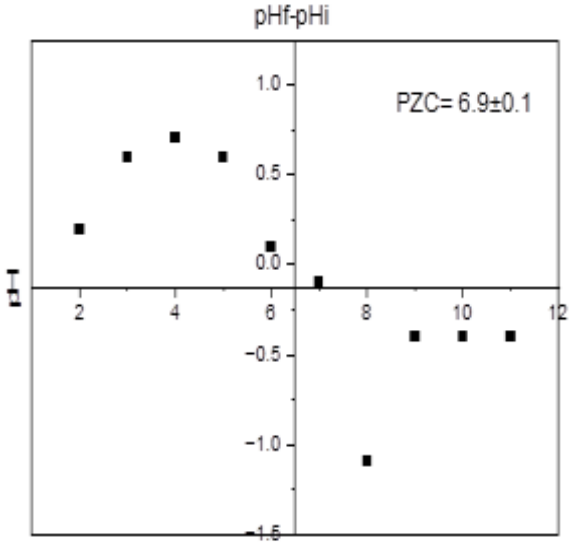

Fig 10: pH_{pzc} analysis of the IONPs

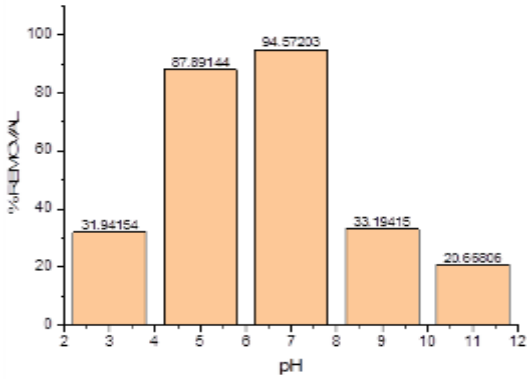

Fig 11: Effect of pH on the removal of ciprofloxacin from water using IONPs

Adsorption isotherm: The experimental results from the adsorption of ciprofloxacin on iron oxide nanoparticles synthesized from orange peel extraction were analyzed. The Langmuir model was found to best fit the data, suggesting that the adsorption occurs on a homogeneous surface with a finite number of identical sites. The Freundlich model's coefficient of correlation (R2) of 0.8757 rejected the hypothesis of multilayer adsorption and heterogeneous distribution of the surface energy. Additionally, the Temkin adsorption model had the least coefficient of correlation (R2), indicating a poor fit with the adsorption mechanism.

Table 1: The adsorption isotherms parameters for the adsorption of ciprofloxacin

Sn	Isotherm	Parameters	OPNPs
1	Langmuir	Qm(mg/g)	29.2056
		KL(l/mg)	3.3404
		RL (mg/l)	0.0184
		R^2	0.9670
2	Freundlich	1/n	0.93400
		N	1.07066
		Kf(mg/g)(l/mg)$^{1/n}$	26.3572
		R^2	0.8757
3	Temkin	RT/b	0.93402
		ln(a)	3.27033
		a(l/g)	26.3200
		b(j/mol)	2653.93
		R^2	0.83432

These findings align with previous research by Azizi (2020) on Fe_3O_4/cellulose magnetic recyclable nanocomposite and Al-Musawi *et al*. (2021) on powdered activated carbon magnetized by iron (III) oxide magnetic nanoparticles (PAC@Fe_3O_4-MN). However, Moradi *et al*. (2016) reported different results for ciprofloxacin adsorption on magnetic metal–organic framework sorbents (MIL-100 (Fe) and MOF-235 (Fe)), while the adsorption of ciprofloxacin on orange peel modified with sodium hydroxide (OP-NaOH) also showed variations (Sadegh *et al*., 2017).The isotherm data were visually represented in

Figures 12(a-c), and the parameters were summarized in Table 1 to provide a comprehensive overview of the experimental findings and their implications.

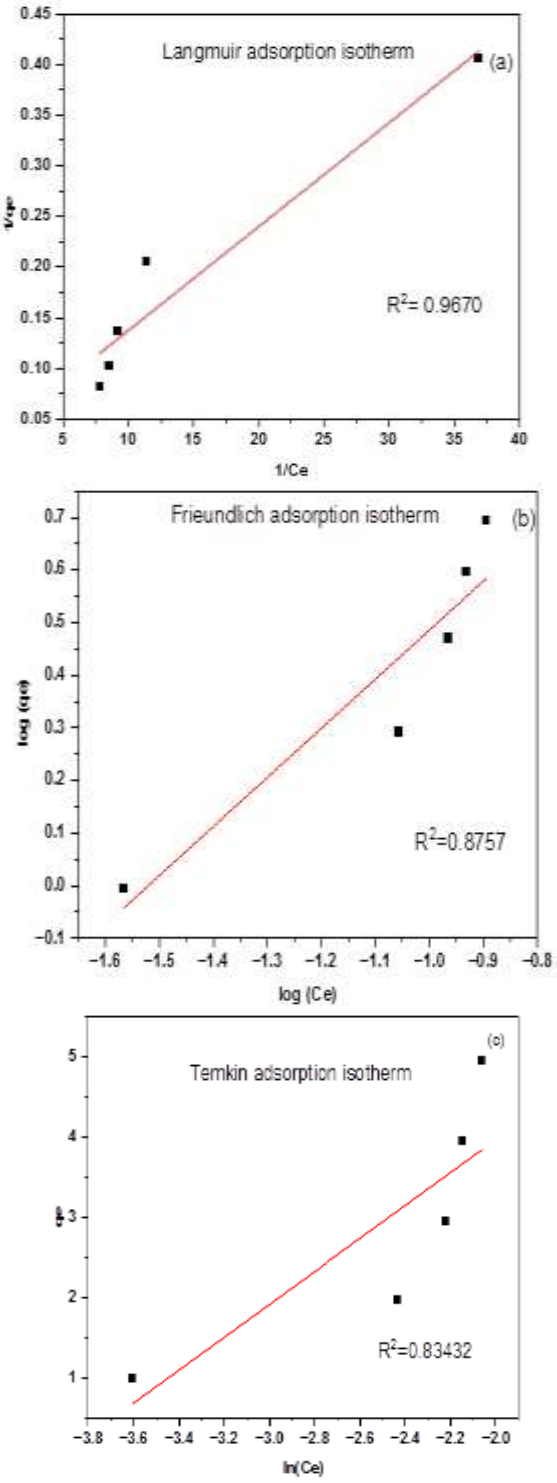

Fig 12: Adsorption isotherm for the adsorption of ciprofloxacin using the synthesized IONPs (a)Langmuir adsorption isotherm (b) Freundlich adsorption isotherm (c) Temkin adsorption isotherm.

Kinetic Study: The analysis of the kinetic model parameters, presented in Table 2, reveals an insight into the adsorption of ciprofloxacin on OPNPs. The pseudo first-order model exhibited a poor fit, as indicated by the negative rate constant (K1) values, suggesting that this model does not effectively describe the adsorption process.

Table 2: Kinetic parameters for Ciprofloxacin adsorption using IONPs

Sn	Kinetic models	Parameters	OPNPs
1	Pseudo 1st order	Qe(mg/g)	2.89938
		K1(mg/g)(l/mg)$^{1/n}$	-0.00037
		R^2	0.90247
2	Pseudo 2nd order	Qe(mg/g)	3.65951
		qe^2	13.39207
		K_2(g/mgs)	0.05129
		R^2	0.96763
3	Intraparticle diffusion	Kp(mg/gmin$^{1/n}$)	0.25025
		C (mg/g)	1.68302
		R^2	0.87032
4	Elovich	α(mg//gmin)	10.1038
		B (g/mg)	2..1256
		R^2	0.75160

Conversely, the pseudo second-order model demonstrated the best fit with the highest R2 value of 0.9967, indicating that the adsorption of ciprofloxacin on OPNPs is primarily controlled by the availability of vacant sites on the adsorbent surface.

Furthermore, the intraparticle diffusion model showed a lower R2 value, implying that factors beyond the diffusion of ciprofloxacin molecules may be influencing the adsorption process, such as electrostatic interactions, pH, and temperature.

The Elovich model also displayed a poor fit, suggesting complex mechanisms at play, including the formation of complexes and surface charge changes. The values of qe2 (13.39 mg/g) and k2 (0.05129 g/mg min) indicate moderate adsorption capacity and relatively fast adsorption rate, both desirable for practical applications.

Additionally, the values of Kp (0.25 mg/g min)1/n and C (1.68 mg/g) suggest a relatively low diffusion rate and low mass transfer resistance.

These findings contribute to a deeper understanding of the adsorption behavior of ciprofloxacin on OPNPs, shedding light on the underlying mechanisms and providing valuable insights for potential practical applications.

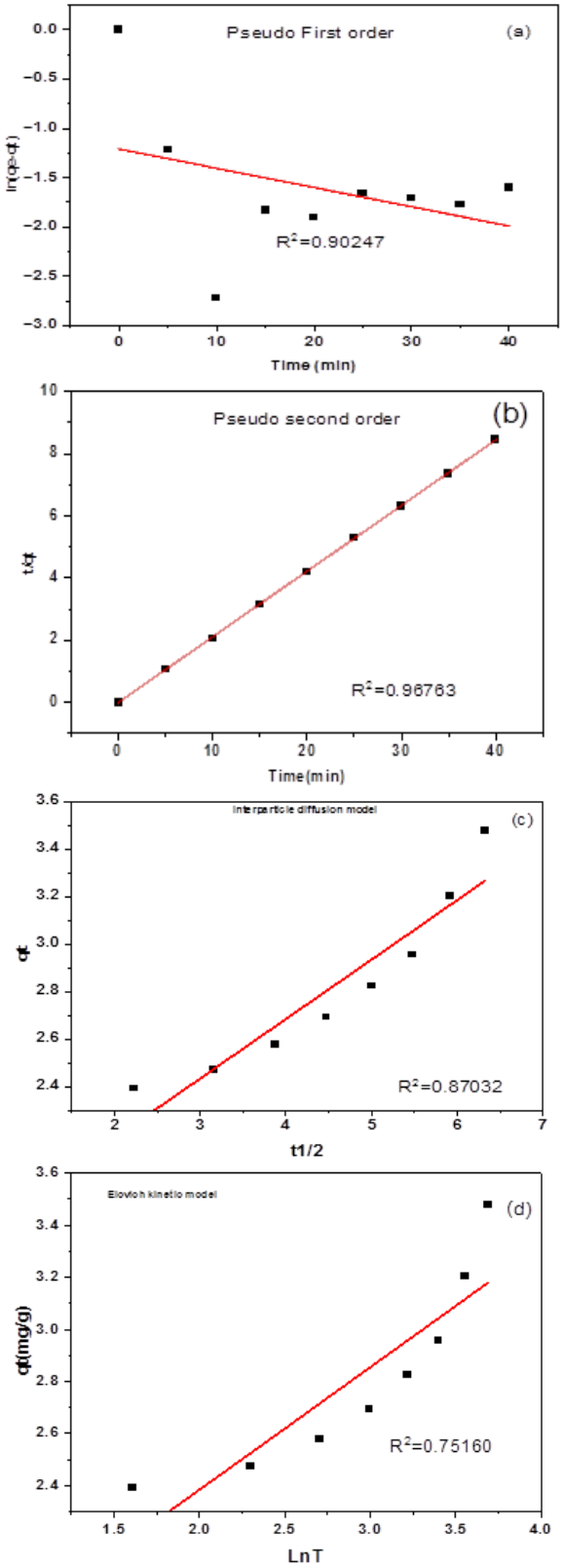

Fig 13: Kinetic models for the adsorption of ciprofloxacin (a) Pseudo first order kinetic model (b) pseudo second Pseudo order kinetic model (c) Interparticle diffusion model (d) Elovich kinetic model.

Conclusion: The paper introduced a sustainable method using orange peel extract to synthesize iron oxide nanoparticles, successfully removing ciprofloxacin from water. The nanoparticles exhibited a nanocrystalline structure, cubic crystal shape, and high thermal stability. The adsorption data aligned well with the Langmuir isotherm and pseudo-second-order kinetic models, indicating monolayer adsorption on a homogeneous surface. At a pH of 7 and 25°C, the maximum adsorption capacity was 29.21 mg/g. The synthesized nanoparticles demonstrated high efficiency and selectivity for eco-friendly water purification.

Conflict of Interest: All the authors, Muhammad, Dahiru Faruruwa, Habib. I. Adamu, Modupe. M. Adeyemi, and Wasiu. B. Tomori declared that there is no conflict of interest attached with this article.

REFERENCES

Adamu, HI; Faruruwa, MD; Adeyemi, MM; Tomori, WB; Akorede, AO. (2023). Plant Synthesized Iron Oxide Nanoparticles for Removal of Emerging Contaminant. *Chem. Afr*, 1-14. https://doi.org/10.1007/s42250-023-00822-0

Ahmadi, M; Monji, D; Taromi, F A. (2021). Bio-inspired surface modification of iron oxide nanoparticles for active stabilization in hydrogels. *Soft Matter*, *17*(4), 955-964.

Ahmadpoor, F; Masood, A; Feliu, N; Parak, W.J; Shojaosadati, S.A.(2021). The effect of surface coating on iron oxide nanoparticles on magnetic resonance imaging relativity. *Front.. Nanotech*, 3, 644734.

Aigbe, UO; Ukhurebor, K E; Onyancha, RB; Okundaye, B; Pal, K., Osibote, OA; Darmokoesoemo, H. (2022). A facile review on the sorption of heavy metals and dyes using bio nanocomposites. *Adsorpt. Sci. Techno*, *2022*, 1-36. https://doi.org/10.1155/2022/8030175

Alangari, A; Alqahtani, MS; Mateen, A; Kalam, MA; Alshememry, A; Ali, R; Syed, R. (2022). Iron oxide nanoparticles: Preparation, characterization, and assessment of antimicrobial and anticancer activity. *Adsorp. Sci. Techno*, *2022*, 1-9. https://doi.org/10.1155/2022/1562051

Al-Musawi, TJ; Mahvi, AH; Khatibi, AD; Balarak, D. (2021). Effective adsorption of ciprofloxacin antibiotic using powdered activated carbon magnetized by iron (III) oxide magnetic nanoparticles. *J. porous mat*, *28*, 835-852. https://doi.org/10.1007/s10934-021-01039-7

Alwared, AI; Al-Musawi, TJ; Muhaisn, L F; Mohammed, AA. (2021). The biosorption of reactive red dye onto orange peel waste: a study on the isotherm and kinetic processes and sensitivity analysis using the artificial neural network approach. *Environ. Sci. Pol. Res. 28*, 2848-2859. https://doi.org/10.1007/s11356-020-10613-6

Arief, S; Muldarisnur, M; Usna, SR. (2023). Enhancement in photoluminescence performance of carbon-based Fe_3O_4@ ZnO–C nanocomposites. *Vacuum*, *211*, 111935. https://doi.org/10.1016/j.vacuum.2023.111935

Aryal, S; Baniya, MK; Danekhu, K; Kunwar, P; Gurung, R; Koirala, N. (2019). Total phenolic content, flavonoid content and antioxidant potential of wild vegetables from Western Nepal. *Plants*, *8*(4), 96. https://doi.org/10.3390/plants8040096

Badawi, AK; Abd Elkodous, M; Ali, GA. (2021). Recent advances in dye and metal ion removal using efficient adsorbents and novel nano-based materials: an overview. *RSC advances*, *11*(58), 36528-36553. DOI: 10.1039/D1RA06892J

Bakatula, EN; Richard, D; Neculita, CM; Zagury, GJ. (2018). Determination of point of zero charge of natural organic materials. *Environ. Sci. Pol. Res*, *25*, 7823-7833. https://doi.org/10.1007/s11356-017-1115-7

Balarak, D; Mahvi, A H; Shim, MJ; Lee, SM. (2021). Adsorption of ciprofloxacin from aqueous solution onto synthesized NiO: isotherm, kinetic and thermodynamic studies. *Desalin Water Treat*, *212*, 390-400.

Bashir, M; Ali, S; Farrukh, MA (2020). Green synthesis of Fe_2O_3 nanoparticles from orange peel extract and a study of its antibacterial activity. *J. Korean Phy. Society*, *76*, 848-854. https://doi.org/10.3938/jkps.76.848

Batool, F; Iqbal, MS; Khan, SU. D; Khan, J; Ahmed, B; Qadir, MI. (2021). Biologically synthesized iron nanoparticles (FeNPs) from Phoenix dactylifera have anti-bacterial activities. *Sci. Rep. 11*(1), 1-9. https://doi.org/10.1038/s41598-021-01374-4

Busetty, S. (2019). Environmental treatment technologies: adsorption. *Handbook of Environ. Mat. Manage*, 1367-1397.

Cheah, P; Brown, P; Qu, J; Tian, B; Patton, DL; Zhao, Y. (2021). Versatile Surface Functionalization of Water-Dispersible Iron Oxide Nanoparticles with Precisely Controlled Sizes. *Langmuir*, *37*(3), 1279-1287. https://doi.org/10.1021/acs.langmuir.0c03314

Checkouri, E; Reignier, F; Robert-Da Silva, C; Meilhac, O. (2020). Evaluation of polyphenol content and antioxidant capacity of aqueous extracts from eight medicinal plants from reunion island: Protection against oxidative stress in red blood cells and preadipocytes. *Antioxidants*, *9*(10), 959. https://doi.org/10.3390/antiox9100959

Chen, T; Liu, Y; Lu, J; Xing, J; Li, J; Liu, T; Xue, Q. (2019). Highly efficient detection of ciprofloxacin in water using a nitrogen-doped carbon electrode fabricated through plasma modification. *New J. Chem*, *43*(38), 15169-15176. https://doi.org/10.3390/antiox9100959

Da'na, E; Taha, A; Afkar, E. (2018). Green synthesis of iron nanoparticles by Acacia nilotica pods extract and its catalytic, adsorption, and antibacterial activities. *App. Sci*, *8*(10), 1922. https://doi.org/10.3390/app8101922

Erukainure, OL; Ebuehi, OA., Choudhary, MI; Mesaik, MA., Shukralla, A; Muhammad, A; Elemo, GN. (2016). Orange peel extracts: Chemical characterization, antioxidant, antioxidative burst, and phytotoxic activities. *J. dietary supp*, *13*(5), 585-594. https://doi.org/10.3109/19390211.2016.1150932

Fahmy, HM; Mohamed, FM; Marzouq, MH; Mustafa, ABED; Alsoudi, A M., Ali, OA; Mahmoud, F. A. (2018). Review of green methods of iron nanoparticles synthesis and applications. *Bio Nano Sci*, *8*, 491-503. https://doi.org/10.1007/s12668-018-0516-5

Faisal, S; Jan, H; Shah, SA; Shah, S;Khan, A;Akbar, MT;Rizwan, M; Jan, F; Wajidullah; Akhtar, N. (2021). Green synthesis of zinc oxide (ZnO) nanoparticles using aqueous fruit extracts of Myristica fragrans: their characterizations and biological and environmental applications. *ACS Omega*, 6(14), 9709–9722. https://doi.org/10.1021/acsomega.1c00310

Gan, PP; Li, SFY. (2012). Potential of plant as a biological factory to synthesize gold and silver nanoparticles and their applications. *Rev. Environ*

Sci Bio/Techno, *11*, 169-206. https://doi.org/10.1007/s11157-012-9278-7

Gao, J; Zheng, X; Meng, Z.; Feng, L. (2022). Adsorption of ciprofloxacin and tetracycline from wastewater by layered double hydroxides modified vermiculite. *J. Por Mat*, *29*(5), 1299-1308. https://doi.org/10.1007/s10934-022-01253-x

Garau, G; Lauro, GP; Diquattro, S; Garau, M; Castaldi, P. (2019). Sb (V) adsorption and desorption onto ferrihydrite: influence of pH and competing organic and inorganic anions. *Environ. J. Sci. Poll. Res*, *26*, 27268-27280. https://doi.org/10.1007/s11356-019-05919-z

Gaumet, M; Vargas, A; Gurny, R; Delie, F. (2008). Nanoparticles for drug delivery: the need for precision in reporting particle size parameters. *Europ.J.pharm.biopharmaceutics*, *69*(1),1-9. https://doi.org/10.1016/j.ejpb.2007.08.001

Hamdaoui, O; Naffrechoux, E. (2007). Modeling of adsorption isotherms of phenol and chlorophenols onto granular activated carbon: Part I. Two-parameter models and equations allowing determination of thermodynamic parameters. *J.haz. mat*, *147*(1-2), 381-394. https://doi.org/10.1016/j.jhazmat.2007.01.021

Harmansah, C; Kutman, MK; Muftuler, FB. (2022). Preparation of iron oxide nanoparticles by banana peels extract and its usage in NDT. *Measurement*, *204*, 11208. https://doi.org/10.1016/j.measurement.2022.112081

Hassabo, AG; Reda, EM; Ghazal, H; Othman, HA. (2023). Synthesis of AgNPs and ZnONPs using tea leaves extract and their utilization to improve dyeability, printability and functionality of cotton and wool fabrics. *Inorg Chem. Comm*, *150*, 110525. https://doi.org/10.1016/j.inoche.2023.110525

Ishak, NM; Kamarudin, SK; Timmiati, SN. (2019). Green synthesis of metal and metal oxide nanoparticles via plant extracts: an overview. *Mat. Res Expr.*, *6*(11), 112004.**_DOI** 10.1088/2053-1591/ab4458

Jadoun, S; Arif, R; Jandid, NK; Meena, RK (2021). Green Synthesis of nanoparticles using plant extracts. A review. *Environ. Chem. Lettters*, 19, 1355-374. https://doi.org/10.1007/s10311-020-01074-x

Jeevanandam, J; Kiew, SF; Boakye-Ansah, S; Lau, SY; Barhoum, A; Danquah, MK; Rodrigues, J. (2022). Green approaches for the synthesis of metal and metal oxide nanoparticles using microbial and plant extracts. *Nanoscale*, *14*(7), 2534-2571. https://doi.org/10.1039/D1NR08144F

Junejo, R; Jalbani, NS; Kaya, S; Serdaroglu, G; Elik, M. (2022). Mathematical modeling studies for the adsorptive removal of ciprofloxacin drug from water samples using functionalized silica resin. *Chem.Papers*, *76*(6), 3413-3423. https://doi.org/10.1007/s11696-022-02085-4

Kalebić, B; Bafti, A; Cajner, H., Marciuš, M; Matijašić, G; Ćurković, L. (2023). Optimization of Ciprofloxacin Adsorption on Clinoptilolite-Based Adsorbents Using Response Surface Methodology. *Nanomat*, *13*(4), 740. https://doi.org/10.3390/nano13040740

Karpagavinayagam, P; Vedhi, C. (2019). Green synthesis of iron oxide nanoparticles using Avicennia marina flower extract. *Vacuum*, *160*, 286-292. https://doi.org/10.1016/j.vacuum.2018.11.043

Khan, S; Bibi, G; Dilbar, S; Ahmad, M; Ali, A; Ullah, Z; Ali, I. (2022). Biosynthesis and characterization of iron oxide nanoparticles from Mentha spicata and screening its combating potential against Phytophthora infestans. *Front. Plant Sci*, *13*, 1001499. https://doi.org/10.3389/fpls.2022.1001499

Kumar, M; Jaiswal, S; Sodhi, KK; Shree, P;Singh, DK; Agrawal, PK; Shukla, P. (2019). Antibiotics bioremediation: perspectives on its ecotoxicity and resistance. *Environ. internat*, *124*, 448-461. https://doi.org/10.1016/j.envint.2018.12.065

Kupina, S; Fields, C; Roman, MC; Brunelle, S L. (2018). Determination of total phenolic content using the Folin-C assay: single-laboratory validation, first action 2017.13. *J. AOAC Internal*, *101*(5), 1466-1472. https://doi.org/10.5740/jaoacint.18-0031

LaGrow, AP; Besenhard, MO; Hodzic, A; Sergides, A; Bogart, LK., Gavriilidis, A; Thanh, NTK. (2019). Unravelling the growth mechanism of the co-precipitation of iron oxide nanoparticles with the

aid of synchrotron X-Ray diffraction in solution. *Nanoscale*, *11*(14), 6620-6628. DOI: 10.1039/c9nr00531e

Lakshmi, CN; Sing, N (2022). Removal of pharmaceutical Compounds: Overview of Treatment methods. In: P. Sing, S., Agarwal, A.K., Gupta., Maliyekkal, S.M (eds) New Trends in Emerging Contaminant. Energy, Environment and Sustainability. Springer, Singapore. https://doi.org/10.1007/978-981-16-8367-1_8.

Lakshminarayanan, S; Shereen, MF; Niraimathi, KL; Brindha, P; Arumugam, A. (2021). One-pot green synthesis of iron oxide nanoparticles from Bauhinia tomentosa: Characterization and application towards synthesis of 1, 3 diolein. *Sci. rep*, *11*(1), 1-13. https://doi.org/10.1038/s41598-021-87960-y

Lamuela-Raventós, RM. (2018). Folin–Ciocalteu method for the measurement of total phenolic content and antioxidant capacity. *Measurement of antioxidant activity & capacity: recent trends appli.*, 107-115. https://doi.org/10.1002/9781119135388.ch6

Latif, MS; Abbas, S; Kormin, F; Mustafa, MK. (2019). Green Synthesis of PlanT-Mediated Metal Nanoparticles: The Role of Polyphenols. *Asian J. Pharmaceut. Clin.Res.*12(7), 75-84. Doi:10.22159/ajpcr. 2019.y12i7.33211. DOI: http://dx.doi.org/10.22159/ajpcr.2019.v12i7.33211

Liang, J; Wu, J; Zeng, Z; Li, M; Liu, W;Zhang, T. (2023). Behavior and mechanisms of ciprofloxacin adsorption on aged polylactic acid and polyethlene microplastics. *Environmental Science and Pollution Research*, *30*(22), 62938-62950. https://doi.org/10.1007/s11356-023-26390-x

Liu, X; Lu, S; Liu, Y; Meng, W; Zheng, B. (2017). Adsorption of sulfamethoxazole (SMZ) and ciprofloxacin (CIP) by humic acid (HA): characteristics and mechanism. *RSC advances*, *7*(80), 50449-50458. DOI: 10.1039/C7RA06231A

Liu, Y.; Zhang, X; Liu, H. (2023). Removal of typical pollutant ciprofloxacin using iron–nitrogen co-doped modified corncob in the presence of hydrogen peroxide. *RSC advances*, *13*(49), 34335-34347. DOI: 10.1039/D3RA06437A

Lunge, S; Singh, S; Sinha, A. (2014). Magnetic iron oxide (Fe_3O_4) nanoparticles from tea waste for arsenic removal. *J. Magnet. Magnet. Mat.*, 19, 21–31. https://doi.org/10.1016/j.jmmm.2013.12.008.

Majumder, A; Ramrakhiani, L; Mukherjee, D (2019) Green synthesis of iron oxide nanoparticles for arsenic remediation in water and sludge utilization. *Clean Techn Environ Policy* 21,795-813. https://doi.org/10.1007/s10098-019-01669-1.

Miri, A; Najafzadeh, H; Darroudi, M; Miri, MJ; Kouhbanani, MAJ; Sarani, M. (2021). Iron oxide nanoparticles: biosynthesis, magnetic behavior, cytotoxic effect. *Chem.Open*, *10*(3), 327-333. **h**ttps://doi.org/10.1002/open.202000186

Mohamed Khalith, SB; Ramalingam, R; Karuppannan, SK; Dowlath, MJ H; Kumar, R; Vijayalakshmi, S; Uma Maheshwari, R; Arunachalam, KD. (2022). Synthesis and characterization of polyphenols functionalized graphitic hematite nanocomposite adsorbent from an agro waste and its application for removal of Cs from aqueous solution. *Chemosphere*, 286(P1), 131493. https://doi.org/10.1016/j.chemosphere.2021.131493.

Moradi, SE; Haji Shabani, AM; Dadfarnia, S; Emami, S. (2016). Effective removal of ciprofloxacin from aqueous solutions using magnetic metal–organic framework sorbents: mechanisms, isotherms and kinetics. *J. Iranian chem. soc*, *13*, 1617-1627. https://doi.org/10.1007/s13738-016-0878-y

Naqvi, SAZ; Irfan, A; Zaheer, S; Sultan, A; Shajahan, S; Rubab, SL; Acevedo, R. (2021). Proximate composition of orange peel, pea peel and rice husk wastes and their potential use as antimicrobial agents and antioxidants. *Vegetos*, *34*, 470-476. https://doi.org/10.1007/s42535-021-00213-1

National Center for Biotechnology Information (2023). PubChem Compound Summary for CID 2764, Ciprofloxacin.RetrievedOctober5,2023from https://pubchem.ncbi.nlm.nih.gov/compound/Ciprofloxacin.

Nawaz, M; Wahab, Z; Rehman, ZU; Bahader, A; Khan, MI;, Uddin, I; Bajaber, MA. (2023). Plant-mediated synthesis of iron oxide nanoparticles/polyvinyl alcohol nanocomposite and exploring their potential adsorption properties against selected heavy metals. *Poly. Bull.*, *80*(7), 7545-7567. https://doi.org/10.1007/s00289-022-04387-9

Ogbezode, JE; Ezealigo, US; Bello, A., Anye, VC; Onwualu, AP (2023) A narrative review of the synthesis characterization and application of iron oxide nanoparticles. *Discover Nano* 18,125. https://doi.org/10.1186/s11671-023-03898-2.

Opotu, LA; Inuwa, IM; Wong, S; Ngadi, N; Razmi, FA. (2022). Errors and inconsistencies in scientific reporting of aqueous phase adsorption of contaminants: a bibliometric study. *Cleaner Materials*, 100100. https://doi.org/10.1016/j.clema.2022.100100

Paul, D; Singhania, A; Das, G. (2022). Catalytic activities of the vaterite and the calcite based solid supported catalysts for spontaneous Fenton-like dye degradation: A comparative study. *J. Environ. Chem. Eng*, *10*(3), 107558.https://doi.org/10.1016/j.jece.2022.107558

Pershina, AG; Brikunova, OY; Perekucha, NA; Demin, AM; Shevelev, OB; Malkeyeva, D; Krasnov, VP. (2020). Supporting data and methods for the characterization of iron oxide nanoparticles conjugated with pH-(low)-insertion peptide, testing their cytotoxicity and analyses of biodistribution in SCID mice bearing MDA-MB231 tumor. *Data. brief*, *29*, 105062. https://doi.org/10.1016/j.dib.2019.105062

Piccin, JS; Dotto, GL; Pinto, LAA. (2011). Adsorption isotherms and thermochemical data of FD&C Red n 40 binding by chitosan. *Brazilian J. Chem. Eng*, *28*, 295-304. https://doi.org/10.1590/S0104-66322011000200014

Priya, Naveen, Kaur, K; Sidhu, AK. (2021). Green synthesis: An eco-friendly route for the synthesis of iron oxide nanoparticles. *Front. Nanotec*, *3*, 655062.https://doi.org/10.3389/fnano.2021.655062

Salgado, P; Márquez, K; Rubilar, O; Contreras, D; Vidal, G. (2019). The effect of phenolic compounds on the green synthesis of iron nanoparticles (Fe x O y-NPs) with photocatalytic activity. *Appl. Nanos*, *9*, 371-385. https://doi.org/10.1007/s13204-018-0931-5

Sharma, M; Yadav, A; Mandal, M K; Dubey, KK. (2022). TiO2 based photocatalysis: a valuable approach for the removal of pharmaceuticals from aquatic environment. *Interna. J. Environ. Sci. Techn*, 1-16. https://doi.org/10.1007/s13762-021-03894-y

Shehata, MG; Awad, TS; Asker, D; El Sohaimy, SA; Abd El-Aziz, NM; Youssef, MM. (2021). Antioxidant and antimicrobial activities and UPLC-ESI-MS/MS polyphenolic profile of sweet orange peel extracts. *Curren.res. food sci*, *4*, 326-33. https://doi.org/10.1016/j.crfs.2021.05.001

Skiba, MI; Vorobyova, VI. (2019). Synthesis of silver nanoparticles using orange peel extract prepared by plasmochemical extraction method and degradation of methylene blue under solar irradiation. *Adv. Mat. Sci. Eng*, *2019*, 1-8. https://doi.org/10.1155/2019/8306015

Soares, SF; Nogueira, J; Trindade, T; Daniel-da-Silva, AL. (2023). Towards efficient ciprofloxacin adsorption using magnetic hybrid nanoparticles prepared with κ-, ι-, and λ-carrageenan. *J. Nanostruc. Chem*, *13*(2), 283-302. https://doi.org/10.1007/s40097-022-00498-x

Song, S; Peng, W; Li, H. (2021). Surface chemistry of mineral adsorbents. *Adsorpt. Nat. Minerals/Water Interfaces*, 55-91.

Subha, V; Divya, K; Gayathri, S; Jagan Mohan, E; Keerthanaa, N; Vinitha, M; Renganathan, S. (2018). Applications of iron oxide nano composite in waste water treatment–dye decolorization and anti–microbial activity. *MOJ Drug Des. Dev. Ther*, *2*, 178-184

Sudhakar, C; Poonkothai, M; Selvankumar, T; Selvam, K. (2022). Facile synthesis of iron oxide nanoparticles using Cassia auriculata flower extract and accessing their photocatalytic degradation and larvicidal effect. J. Mater. Sci. Mater. Electron. 33, 11434–11445. https://doi: 10.1007/s10854-022-08116-w

Thai, T; Salisbury, BH; Zito, PM. (2023). Ciprofloxacin. In *StatPearls [Internet]*. StatPearls Publishing.

Thi, TUD; Nguyen, TT; Thi, YD; Thi, KHT; Phan, BT; Pham, KN. (2020). Green synthesis of ZnO nanoparticles using orange fruit peel extract for antibacterial activities. *RSC advances*, *10*(40), 23899-23907. DOI: 10.1039/D0RA04926C

Uruén, C; Chopo-Escuin, G; Tommassen, J; Mainar-Jaime, RC; Arenas, J. (2020). Biofilms as promoters of bacterial antibiotic resistance and

tolerance. *Antibiotics*, *10*(1), 3. https://doi.org/10.3390/antibiotics10010003

Wakejo, WK; Meshasha, BT; Kang, JW; Chebude, Y. (2022). Enhanced ciprofloxacin removal from aqueous solution using a chemically modified biochar derived from bamboo sawdust: adsorption process optimization with response surface methodology. *Adsorp. Sci. Techno*, *2022*. https://doi.org/10.1155/2022/2699530

Yang, SH; Yan, L; Huang, XF; Wang, SG. (2020). Adsorption behavior and mechanism of ciprofloxacin from aqueous solution onto magnetic graphene oxide nanocomposite. Front. Environ.Sci. Eng., 14(6), 1–13.

Yau, XH; Liu, WW; Ooi, ZX; Teoh, YP. (2017). Direct synthesis iron oxide nanoparticles using ramie, lemon and dragon fruit as green and low-cost approach. *J. Fundame. Appl. Sci*, *9*(6S), 1-15.

Yew, YP; Shameli, K; Miyake, M; Kuwano, N; Bt Ahmad Khairudin, NB; Bt Mohamad, SE; Lee, KX. (2016). Green synthesis of magnetite (Fe_3O_4) nanoparticles using seaweed (Kappaphycus alvarezii) extract. *Nanoscale research letters*, *11*(1), 1-7 https://doi.org/10.1186/s11671-016-1498-2

Zambri, NDS; Taib, NI; Abdul Latif, F; Mohamed, Z. (2019). Utilization of neem leaf extract on biosynthesis of iron oxide nanoparticles. *Molecules*, *24*(20), 3803. https://doi.org/10.3390/molecules24203803

Zayed, M; Ghazal, H; Othman, HA; Hassabo, AG. (2022). Synthesis of different nanometals using Citrus Sinensis peel (orange peel) waste extraction for valuable functionalization of cotton fabric. *Chemical Papers*, 1-22. https://doi.org/10.1007/s11696-021-01881-8

Zhang, T; Liu, Y; Rao, Y; Li, X; Yuan, D; Tang, S; Zhao, Q. (2020). Enhanced photocatalytic activity of TiO2 with acetylene black and persulfate for degradation of tetracycline hydrochloride under visible light. *Chemi.Engin. J*, *384*, 123350. https://doi.org/10.1016/j.cej.2019.123350